Supplement of Atmos. Chem. Phys., 20, 5513–5526, 2020
https://doi.org/10.5194/acp-20-5513-2020-supplement

Atmospheric Chemistry and Physics
Open Access
EGU

Supplement of

Partitioning of hydrogen peroxide in gas-liquid and gas-aerosol phases

Xiaoning Xuan et al.

Correspondence to: Zhongming Chen (zmchen@pku.edu.cn)

The experimental conditions of the extracted solution

The extracted solution was stored under refrigeration at 255 K, away from light. The first reason to choose 255 K was that the temperature during BJ-2018Winter measurement averaged 270 K, less than 273 K. The second reason was that under 255 K, the decomposition rate of H_2O_2 should be reduced, which contributed to a more accurate estimation of the decomposition rates of organic peroxides to H_2O_2. Li et al. (2016) studied the stability of H_2O_2 in SOA stored on-filter at 255 K and 298 K. It was found that the level of H_2O_2 remained stable for 6 days at 255 K but decreased gradually at 298 K. The third reason was that the H_2O_2 level in the extracted solution was very low at time=0, which could easily decompose at 277 K; therefore, the extracted solution should be stored at 255 K.

Due to the positive correlation between temperature and decomposition rates, the derived rates of decomposition in this paper were lower than the actual rates of decomposition. To discuss the influence of the storage temperature on the decomposition rates of organic peroxides, hydroxymethyl hydroperoxide (HMHP), peroxyformic acid (PFA), and peroxyacetic acid (PAA) were chosen as representatives. According to the Arrhenius equation, the reaction rate usually increases exponentially as temperature increases. The ratios of the decomposition/hydrolysis rates of HMHP, PFA, and PAA at 270 K to 255 K were 13, 3, and 2, respectively (Zhou and Lee, 1992; Dul'neva and Moskvin, 2005; Sun et al., 2011). We have considered the influence of temperature on the decomposition rates of organic peroxides when calculating the aerosol-phase H_2O_2 formation rate from the decomposition/hydrolysis of organic peroxides, as shown in Sec. 3.3 in the Text.

The extracted solution was away from light in this paper, which was different from atmospheric relevant conditions (i.e., exposure to sunlight in the ambient atmosphere), and may affect the data applicability in this study. We chose this experimental condition because if the extracted solution is exposed to sunlight, the photochemical reactions of organic matters and the decomposition/hydrolysis of organic peroxides will coexist, and

we cannot distinguish the effects of these two processes. By doing so, the specific contribution of the decomposition/hydrolysis of organic peroxides to the aerosol-phase H_2O_2 was estimated. With respect to the photochemical reactions of organic matters, Zhou et al. (2008) have discussed that as the exposure time of the extracted solution to sunlight increased, the production of peroxides in nascent marine aerosols first increased rapidly and then slowly. The change trend in Zhou's study was the same as that of the aerosol-phase H_2O_2 level in this paper (Fig. 6). The estimated 24-h-average rate of H_2O_2 photochemical production in Alert particles was about 9 mM h^{-1} at 248 K (Anastasio and Jordan, 2004). We assumed that the photoformation rate of H_2O_2 in Beijing particles was also 9 mM h^{-1}. And the concentrations of aerosol water content (AWC) and $PM_{2.5}$ from 2 January to 3 January 2019 were 3.20 μg m^{-3} and 90.36 μg m^{-3}, respectively. The formation rate of the aerosol-phase H_2O_2 from photochemical reactions was estimated to be 0.011 ng μg^{-1} h^{-1} at 248 K. In addition, the activation energy of H_2O_2 photoformation was 9 kJ mol^{-1} (Anastasio et al., 1994), and the rate of H_2O_2 photoformation at 270 K should be 1.4 times higher than the value at 248 K. Compared with the aerosol-phase H_2O_2 formation rates from the decomposition/hydrolysis of organic peroxides and the heterogeneous uptake of HO_2, the H_2O_2 photoformation could be neglected.

Based on the above analysis, we believe that the derived rates of decomposition under the experimental conditions in this paper can be applied to the ambient atmosphere.

Adsorption experiments of aerosol-phase H_2O_2 on Teflon filters

It is apparent that H_2O_2 is a polar molecule with hydrogen bond, and it has the advantage of strong oxidation. So H_2O_2 stands a good chance at adsorbing on the filters. To evaluate the amount of H_2O_2 adsorbed on the particle-free Teflon filters, we collected 18 adsorption samples in nine days using the second filter placed after the first filter. The particle-trapped efficiency in the first filter was close to ~ 100 %, thereby avoiding the adsorption interference from aerosols in the second filter. Half of the samples had no detectable H_2O_2, while the concentration of H_2O_2 in other samples varied from 0.01

μM to 0.03 μM in the extracted solution of 10 mL H_3PO_4, as shown in Fig. S1. The average of all the adsorption samples was about 0.01 μM, accounting for 15 % of the measured aerosol-phase H_2O_2 concentration. The adsorption experiments verify that H_2O_2 is originated from aerosols, rather than from reactions between ambient air species with the filters (Hewitt and Kok, 1991).

Calculating the residual H_2O_2 in raindrops

$$Sh = 2 + 0.6Re^{1/2}Sc^{1/3} \quad \text{(S1)}$$

$$Sh = \frac{D_P k_g}{D} \quad \text{(S2)}$$

$$Re = \frac{uD_P}{v} \quad \text{(S3)}$$

$$Sc = \frac{v}{D} \quad \text{(S4)}$$

$$C_{aq}^{d} = C_g^m H_A^t - (C_g^m H_A^t - C_{aq}^0)\exp(-\frac{6k_g Z}{D_P u H_A^t R T_S}) \quad \text{(S5)}$$

Where D_P is the equivalent raindrops diameter, cm; u is the terminal fall velocity of a raindrop, cm s^{-1} (Gunn and Kinzer, 1949); Sh is the Sherwood number, dimensionless; Re is the Reynolds number, dimensionless; Sc is the Schmidt number, dimensionless; k_g is the gas-phase mass transfer coefficient, cm s^{-1} (Adamowicz, 1979); D is the diffusivity of H_2O_2 in the air, 0.186 cm^2 s^{-1}; v is the kinematic viscosity of air, 0.133 cm^2 s^{-1}; C_{aq}^{d} is the concentration of liquid-phase H_2O_2 in raindrops at the ground (Levine and Schwartz, 1982; Seinfeld and Pandis, 2006), μM; C_{aq}^0 is the concentration of liquid-phase H_2O_2 in cloud water, μM; C_g^m is the averaged concentration of H_2O_2 in the gas phase, 2.98×10^{-10} atm; H_A^t is the theoretical Henry's law constant of H_2O_2, 8.4×10^4 M atm^{-1} in pure water at 298 K; Z is the fall distance, m; R is the gas constant, 0.082 L atm K^{-1} mol^{-1}, and T_S is the average temperature on rainy days during BJ-2018Summer, 298 ± 2 K (mean ± standard deviation, the same hereafter).

Comparison with aerosol-phase H_2O_2 level in previous studies

The average concentration of aerosol-phase H_2O_2 in this study was 0.093 ± 0.085 ng μg^{-1}, which was a fifth of 0.50 ± 0.30 ng μg^{-1} in Los Angeles (Arellanes et al., 2006) and 0.49 ± 0.55 ng μg^{-1} in Riverside (Wang et al., 2012). Only in one study (Wang et al., 2012), the mean level of H_2O_2 in aerosols (0.11 ± 0.07 ng μg^{-1}) was close to that in this paper. Details are presented in Table S3. This could be explained as follows.

First, in the studies of Hung and Wang (2001), Venkatachari et al. (2005) and Khurshid et al. (2014), the aerosol-phase concentration of reactive oxygen species (ROS) was measured, including H_2O_2, OH radical and other species, thus higher concentration was observed. In addition, the sonication or ultrasonication methods used were found to produce H_2O_2 in purified water, also partially explaining the higher concentration observed (Arellanes et al., 2006). Second, the extraction time imposed a crucial influence on the concentration of aerosol-phase H_2O_2. It has been demonstrated that the concentration of H_2O_2 was positively associated with extraction time, due to the decomposition/hydrolysis of several other compounds in the aerosol phase (Hewitt and Kok, 1991; Li et al., 2016). The extraction time in this study was 15 min, compared with 2 h or 4 h in previous studies (Arellanes et al., 2006; Wang et al., 2010; Shen et al., 2011; Wang et al., 2012). We used a shaker to extract the aerosol-phase H_2O_2, which has already been confirmed that the extraction efficiency could be up to 97 % with 15 min (Li et al., 2016). Thus, the extraction time should be short to avoid the decomposition/hydrolysis of certain compounds (e.g., organic peroxides) in the aerosol phase to form additional of H_2O_2 in the extracted solution. Third, the concentration of SO_2 was higher in China than that in the United States. Higher concentration of SO_2 may consume more aerosol-phase H_2O_2, leading to the lower level of H_2O_2 in aerosols in this study. Fourth, pH in aerosols in China was higher than that in the United States (Liu et al., 2017), also providing part of explanations to the lower level of aerosol-phase H_2O_2 in China, because H_2O_2 was easy to decompose under weak acid conditions.

Calculating the contribution of aerosol-phase H_2O_2 to sulfate formation in a severe haze event

We used the thermodynamic model ISORROPIA-II (Guo et al., 2015) to estimate AWC based on RH, temperature, the measured cations (Na^+, NH_4^+, K^+, Mg^{2+}, and Ca^{2+}), and anions (Cl^-, NO_3^-, and SO_4^{2-}) levels. The RH during BJ-2018Winter (5−35 %) was lower than that of previous studies. Because the ISORROPIA-II model has large errors at low RH (Bian et al., 2014), so we calculate AWC during haze events accompanied by high RH, e.g., a heavy haze episode from 2 January to 3 January 2019.

To our knowledge, there are numerous oxidants in the fast growth of SO_4^{2-} on haze days, including H_2O_2, O_3, transition metals, ROOH, and so on. H_2O_2, as a major oxidant in acidic conditions (Hoffmann and Edwards, 1975), has great opportunities to oxidize SO_2 into SO_4^{2-} during heavy haze pollution. Because the level of aerosol-phase H_2O_2 was higher than the predicted value using gas-aerosol partitioning, we should pay more attention to the measured level of H_2O_2 in the aerosol phase, and reevaluated the important contribution of H_2O_2 to SO_4^{2-} formation. We calculated the reaction rate (RR) and the sulfate formation rate (SFR) during a heavy haze episode. Given that pH is around 5 in aerosols consistent with recent studies (Liu et al., 2017; Ye et al., 2018), the results are listed in Table S4.

In this study, during a heavy haze episode from 2 January to 3 January 2019, the average level of SO_2 was 6.74 ppbv, and the levels of field-measured H_2O_2 in the gas and aerosol phases were 16.94 pptv and 6.87×10^3 μM, respectively. Based on the measured H_2O_2, the mean RR and SFR were around 3.03×10^{-3} μmol m^{-3} h^{-1} and 0.29 μg m^{-3} h^{-1}, which were three orders of magnitude higher than calculated by predicted H_2O_2. Moreover, the growth rate of SO_4^{2-} calculated was 0.51 μg m^{-3} h^{-1}, and the H_2O_2 oxidation pathway contributed to about 57 % of the measured growth of SO_4^{2-}. The result strongly suggested that H_2O_2 acted as the main oxidant in the formation of sulfate, and might play vital roles in the rapid growth of $PM_{2.5}$ during sever haze pollution.

In this study, the ratio of mass concentrations of SO_4^{2-} to $PM_{2.5}$ was 6 %, which was lower than that in previous studies. The ratio in Beijing was 19 % in 2013 (Ho et al.,

2016), and decreased to around 10 % in 2016−2017 (Shao et al., 2018; Xu et al., 2019). We suggested that the continued decline of the ratio in 2018 was due to the strict control of SO_2 emission. As a matter of fact, NO_3^- gradually dominated the mass concentration of $PM_{2.5}$ (Xu et al., 2019). Next, the analysis method of SO_4^{2-} in this paper was offline filter-based measurement. The method had a good agreement but was lower than the online measurement (Zhang et al., 2019). In addition, the SO_4^{2-} data was the average during the 11.5 h sampling period, which may underestimate the growth rate of SO_4^{2-}. All the reasons mentioned could be responsible for the decrease in the ratio of SO_4^{2-} to $PM_{2.5}$.

Heterogeneous uptake of H_2O_2 on aerosols

$$\gamma = \frac{5.32 \times 10^{-5}}{1 - 0.82 \times (RH/100)^{0.13}} \quad \text{(S6)}$$

$$\gamma = \frac{d[X]_p^{t,h}/dt}{Z} \quad \text{(S7)}$$

$$Z = \frac{1}{4}\omega S_{aw}[X]_g \quad \text{(S8)}$$

$$\omega = \sqrt{\frac{8RT_W}{\pi M_X}} \quad \text{(S9)}$$

$$S_{aw} = S_a \times f(RH) = S_a \times [1 + a(RH/100)^b] \quad \text{(S10)}$$

$$[X]_p^{t,h} = \int_0^t \frac{d[X]_p^{t,h}}{dt} \quad \text{(S11)}$$

Where γ is the heterogeneous uptake coefficient, dimensionless; $[X]_p^{t,h}$ is the net heterogeneous uptake of gas-phase H_2O_2 on aerosols, molecules; Z is the collision frequency between gas-phase H_2O_2 and aerosols' surface, molecules s^{-1}; ω is the average movement rate of gas-phase H_2O_2, m s^{-1}; S_{aw} is the surface area of aerosols, m^2; $f(RH)$ is the hygroscopic factor, dimensionless; a and b are experience factors (a=8.8, b=9.7, Liu et al., 2013). Due to low RH in the BJ-2018Winter measurement, we did not consider the effect of RH on the surface area. Since the average $PM_{2.5}$ mass concentration was 39.21 μg m^{-3} during the entire measurement period and 31.10 μg

m^{-3} on clean days, the aerosol surface area concentration was assumed to be 400 μm^2 cm^{-3} (Kuang et al., 2019); $[X]_g$ is the concentration of gas-phase H_2O_2, molecules m^{-3}; M_X is the average molar mass of gas-phase H_2O_2, kg mol^{-1}; R is the ideal gas constant, 8.314 Pa m^3 K^{-1} mol^{-1}; T_W is the actual temperature during BJ-2018Winter, 270 K. Subsequently, we could figure out the average heterogeneous uptake rate of H_2O_2 on aerosols based on Eqs. (S6) to (S11) (Wu et al., 2015).

The influence of the extraction and transportation processes on the effective gas-aerosol partitioning coefficient

It took around 40 min to extract and transport the sample to the observation site for H_2O_2 measurement. Organic peroxides in the extracted solution may decompose into H_2O_2 during the process, leading to overestimation of the effective gas-aerosol partitioning coefficient of H_2O_2. Provided that the maximum decomposition/hydrolysis rate of organic peroxides was 0.10 ng μg^{-1} h^{-1}, the corrected gas-aerosol partitioning coefficient averaged 6.9×10^{-4} m^3 μg^{-1}, which was the lowest value due to the assumed maximum value of the decomposition/hydrolysis rate of organic peroxides. Because the corrected value of the effective gas-aerosol partitioning coefficient was much higher than K_P^t, we did not correct the data.

Calculating the reaction rates between H_2O_2 or O_3 and S(IV)

$$-\frac{d[S(IV)]}{dt} = (k_0[SO_2 \cdot H_2O] + k_1[HSO_3^-] + k_2[SO_3^{2-}])[O_3] \quad \text{(S12)}$$

$$-\frac{d[S(IV)]}{dt} = \frac{7.5 \times 10^7 [H^+][HSO_3^-][H_2O_2]}{1 + 13[H^+]} \quad \text{(S13)}$$

Where k_0, k_1 and k_2 are the rate constants of reactions between O_3 and S(IV); $[O_3]$ and $[H_2O_2]$ are the liquid-phase levels of O_3 and H_2O_2; $[SO_2 \cdot H_2O]$, $[HSO_3^-]$ and $[SO_3^{2-}]$ are the concentrations of S(IV) species in the liquid phase.

The influence of transition metals on the aerosol-phase H_2O_2 level

It is demonstrated that Fe and Cu (measured using ICP-MS) have small effects on the

level of aerosol-phase H_2O_2 (Fig. S6), similar to the results of previous studies (Tummala, 2015). It is suggested that transition metals might not account for the majority formation of H_2O_2 in ambient aerosols in Beijing, instead other physical and chemical reactions play major parts in that, as stated in the Text.

Figure caption.

Table S1: Detection rates and concentrations of peroxides in the liquid and gas phases.

Table S2: The differences between the measured (C_{aq}^{m}) and predicted (C_{aq}^{t}) liquid-phase H_2O_2 levels for the three types of seven rain events.

Table S3: Summary of aerosol-phase H_2O_2 concentration in previous studies.

Table S4: The estimated averages of reaction rate (RR) and sulfate formation rate (SFR) during a sever haze event on 2−3 January 2019.

Table S5: The ratio of the maximum to initial H_2O_2 concentration (C_{max}/C_0) in the extracted solution and molar concentration ratio of aerosol-phase TPOs to H_2O_2 for the three types.

Table S6: The average values of meteorological parameters, trace gases, $PM_{2.5}$ and TPOs for the three types during BJ-2018Winter.

Figure S1: The concentrations of H_2O_2 in adsorption and aerosol samples in the extracted solution from 27 December 2018 to 4 January 2019.

Figure S2: Concentrations of the measured (a) gas-phase and (b) liquid-phase H_2O_2 in seven rain episodes during BJ-2018Summer.

Figure S3: The variation of effective field-derived Henry's law constant (H_A^m) with temperature in seven rain episodes.

Figure S4: The relationship between the measured liquid-phase H_2O_2 level (left axis) or rain intensity (right axis) and time on 1−2 September 2018.

Figure S5: Measured concentrations of (a) gas-phase and (b) aerosol-phase H_2O_2 during BJ-2018Winter.

Figure S6: The dependency of measured H_2O_2 concentration on levels of (a) Cu and (b) Fe in aerosols.

References

Adamowicz, R. F.: A model for the reversible washout of sulfur-dioxide, ammonia and carbon-dioxide from a polluted atmosphere and the production of sulfates in raindrops, Atmos. Environ., 13, 105−121, https://doi.org/10.1016/0004-6981(79)90250-6, 1979.

Anastasio, C., Faust, B. C., and Allen, J. M.: Aqueous phase photochemical formation of hydrogen peroxide in authentic cloud waters, J. Geophys. Res., 99, 8231−8248, https://doi.org/10.1029/94JD00085, 1994.

Anastasio, C., and Jordan, A. L.: Photoformation of hydroxyl radical and hydrogen peroxide in aerosol particles from Alert, Nunavut: implications for aerosol and snowpack chemistry in the Arctic, Atmos. Environ., 38, 1153−1166, https://doi.org/10.1016/j.atmosenv.2003.11.016, 2004.

Arellanes, C., Paulson, S. E., Fine, P. M., and Sioutas, C.: Exceeding of Henry's law by hydrogen peroxide associated with urban aerosols, Environ. Sci. Technol., 40, 4859−4866, https://doi.org/10.1021/es0513786, 2006.

Bian, Y. X., Zhao, C. S., Ma, N., Chen, J., and Xu, W. Y.: A study of aerosol liquid water content based on hygroscopicity measurements at high relative humidity in the North China Plain, Atmos. Chem. Phys., 14, 6417–6426, https://doi.org/10.5194/acp-14-6417-2014, 2014.

Dul'neva, L. V. and Moskvin, A. V.: Kinetics of formation of peroxyacetic acid, Russ. J. Gen. Chem., 75, 1125−1130, https://doi.org/10.1007/s11176-005-0378-8, 2005.

Gunn, R. and Kinzer, G. D.: The terminal velocity of fall for water droplets in stagnant air, J. Meteorol., 6, 243−248, https://doi.org/10.1175/1520-0469(1949)006<0243:TTVOFF>2.0.CO;2, 1949.

Guo, H., Xu, L., Bougiatioti, A., Cerully, K. M., Capps, S. L., Hite Jr., J. R., Carlton, A. G., Lee, S.-H., Bergin, M. H., Ng, N. L., Nenes, A., and Weber, R. J.: Fine-particle water and pH in the southeastern United States, Atmos. Chem. Phys., 15, 5211–5228, https://doi.org/10.5194/acp-15-5211-2015, 2015.

Hasson, A. S. and Paulson, S. E.: An investigation of the relationship between gas-phase and aerosol-borne hydroperoxides in urban air, J. Aerosol. Sci., 34, 459−468,

https://doi.org/10.1016/S0021-8502(03)00002-8, 2003.

Hewitt, C. N. and Kok, G. L.: Formation and occurrence of organic hydroperoxides in the troposphere: laboratory and field observations, J. Atmos. Chem., 12, 181−194, https://doi.org/10.1007/Bf00115779, 1991.

Ho, K. F., Ho, S. S. H., Huang, R. J., Chuang, H. C., Cao, J. J., Han, Y. M., Lui, K. H., Ning, Z., Chuang, K. J., Cheng, T. J., Lee, S. C., Hu, D., Wang, B., and Zhang, R. J.: Chemical composition and bioreactivity of $PM_{2.5}$ during 2013 haze events in China, Atmos. Environ., 126, 162−170, https://doi.org/10.1016/j.atmosenv.2015.11.055, 2016.

Hoffmann, M. R. and Edwards, J. O.: Kinetics of the oxidation of sulfite by hydrogen peroxide in acidic solution, J. Phys. Chem., 79, 2096−2098, https://doi.org/10.1021/j100587a005, 1975.

Hung, H. F. and Wang, C. S.: Experimental determination of reactive oxygen species in Taipei aerosols, J. Aerosol. Sci., 32, 1201−1211, https://doi.org/10.1016/S0021-8502(01)00051-9, 2001.

Khurshid, S. S., Siegel, J. A., and Kinney, K. A.: Technical Note: particulate reactive oxygen species concentrations and their association with environmental conditions in an urban, subtropical climate, Atmos. Chem. Phys., 14, 6777−6784, https://doi.org/10.5194/acp-14-6777-2014, 2014.

Kuang, Y., Tao, J. C., Xu, W. Y., Yu, Y. L., Zhao, G., Shen, C. Y., Bian, Y. X., and Zhao, C. S.: Calculating ambient aerosol surface area concentrations using aerosol light scattering enhancement measurements, Atmos. Environ., 216, 116919, https://doi.org/10.1016/j.atmosenv.2019.116919, 2019.

Levine, S. Z. and Schwartz, S. E.: In-cloud and below-cloud scavenging of nitric acid vapor, Atmos. Environ., 16, 1725−1734, https://doi.org/10.1016/0004-6981(82)90266-9, 1982.

Li, H., Chen, Z. M., Huang, L. B., and Huang, D.: Organic peroxides' gas-particle partitioning and rapid heterogeneous decomposition on secondary organic aerosol, Atmos. Chem. Phys., 16, 1837−1848, https://doi.org/10.5194/acp-16-1837-2016, 2016.

Liu, M. X., Song, Y., Zhou, T., Xu, Z. Y., Yan, C. Q., Zheng, M., Wu, Z. J., Hu, M., Wu, Y. S., and Zhu, T.: Fine particle pH during severe haze episodes in northern China, Geophys. Res. Lett., 44, 5213−5221, https://doi.org/10.1002/2017GL073210, 2017.

Liu, X. G., Gu, J. W., Li, Y. P., Cheng, Y. F., Qu, Y., Han, T. T., Wang, J. L., Tian, H. Z., Chen, J., and Zhang, Y. H.: Increase of aerosol scattering by hygroscopic growth: observation, modeling, and implications on visibility, Atmos. Res., 132−133, 91−101, https://doi.org/10.1016/j.atmosres.2013.04.007, 2013.

Seinfeld, J. H. and Pandis S. N.: Atmospheric chemistry and physics: from air pollution to climate change, 2nd Edition, John Wiley and Sons, New Jersey, the United States of America, 2006.

Shao, P. Y., Tian, H. Z., Sun, Y. J., Liu, H. J., Wu, B. B., Liu, S. H., Liu, X. Y., Wu, Y. M., Liang, W. Z., Wang, Y., Gao, J. J., Xue, Y. F., Bai, X. X., Liu, W., Lin, S. M., and Hu, G. Z.: Characterizing remarkable changes of severe haze events and chemical compositions in multi-size airborne particles (PM_1, $PM_{2.5}$ and PM_{10}) from January 2013 to 2016−2017 winter in Beijing, China, Atmos. Environ., 189, 133−144, https://doi.org/10.1016/j.atmosenv.2018.06.038, 2018.

Shen, H., Barakat, A. I., and Anastasio, C.: Generation of hydrogen peroxide from San Joaquin Valley particles in a cell-free solution, Atmos. Chem. Phys., 11, 753−765, https://doi.org/10.5194/acp-11-753-2011, 2011.

Sun, X. Y., Zhao, X. B., Du, W., and Liu, D. H.: Kinetics of formic acid-autocatalyzed preparation of performic acid in aqueous phase, Chin. J. Chem. Eng., 19, 964−971, https://doi.org/10.1016/S1004-9541(11)60078-5, 2011.

Tummala, S. K.: Investigation of the sources of hydrogen peroxide in ambient particulate matter, Master thesis, California State University, the United States of America, 2015.

Venkatachari, P., Hopke, P. K., Grover, B. D., and Eatough, D. J.: Measurement of particle-bound reactive oxygen species in Rubidoux aerosols, J. Atmos. Chem., 52, 325−326, https://doi.org/10.1007/s10874-005-1662-z, 2005.

Wang, Y., Arellanes, C., Curtis, D. B., and Paulson, S. E.: Probing the source of hydrogen peroxide associated with coarse mode aerosol particles in southern

California, Environ. Sci. Technol., 44, 4070−4075, https://doi.org/10.1021/es100593k, 2010.

Wang, Y., Arellanes, C., and Paulson, S. E.: Hydrogen peroxide associated with ambient fine-mode, diesel, and biodiesel aerosol particles in southern California, Aerosol Sci. Tech., 46, 394−402, https://doi.org/10.1080/02786826.2011.633582, 2012.

Wu, Q. Q., Huang, L. B., Liang, H., Zhao, Y., Huang, D., and Chen, Z. M.: Heterogeneous reaction of peroxyacetic acid and hydrogen peroxide on ambient aerosol particles under dry and humid conditions: kinetics, mechanism and implications, Atmos. Chem. Phys., 15, 6851−6866, https://doi.org/10.5194/acp-15-6851-2015, 2015.

Xu, Q. C., Wang, S. X., Jiang, J. K., Bhattarai, N., Li, X. X., Chang, X., Qiu, X. H., Zheng, M., Hua, Y., and Hao, J. M.: Nitrate dominates the chemical composition of $PM_{2.5}$ during haze event in Beijing, China, Sci. Total Environ., 689, 1293−1303, https://doi.org/10.1016/j.scitotenv.2019.06.294, 2019.

Ye, C., Liu, P. F., Ma, Z. B., Xue, C. Y., Zhang, C. L., Zhang, Y. Y., Liu, J. F., Liu, C. T., Sun, X., and Mu, Y. J.: High H_2O_2 concentrations observed during haze periods during the winter in Beijing: importance of H_2O_2 oxidation in sulfate formation, Environ. Sci. Technol. Lett., 5, 757−763, https://doi.org/10.1021/acs.estlett.8b00579, 2018.

Zhang, B. Y., Zhou, T., Liu, Y., Yan, C. Q., Li, X. Y., Yu, J. T., Wang, S. X., Liu, B. X., and Zheng, M.: Comparison of water-soluble inorganic ions and trace metals in $PM_{2.5}$ between online and offline measurements in Beijing during winter, Atmos. Pollut. Res., 10, 1755−1765, https://doi.org/10.1016/j.apr.2019.07.007, 2019.

Zhou, X. L., Davis, A. J., Kieber, D. J., Keene, W. C., Maben, J. R., Maring, H., Dahl, E. E., Izaguirre, M. A., Sander, R., and Smoydzyn, L.: Photochemical production of hydroxyl radical and hydroperoxides in water extracts of nascent marine aerosols produced by bursting bubbles from Sargasso seawater, Geophys. Res. Lett., 35, L20803, https://doi.org/10.1029/2008GL035418, 2008.

Zhou, X. L., and Lee, Y. N.: Aqueous solubility and reaction kinetics of hydroxymethyl hydroperoxide, J. Phys. Chem., 96, 265−272, https://doi.org/10.1021/j100180a051, 1992.

Table S1: Detection rates and concentrations of peroxides in the liquid and gas phases.

Phases	Peroxides	Mean ± S.D. (μM)	Detection rate (%)
Liquid phase	H_2O_2	44.12 ± 26.49	100
	HMHP[a]	0.23 ± 0.13	42
	MHP[b]	0.41 ± 0.25	78
Gas phase	H_2O_2	0.30 ± 0.26	100
	MHP	0.34 ± 0.03	6
	PAA[c]	0.02 ± 0.01	54

[a] HMHP is hydroxymethyl hydroperoxide.

[b] MHP is methyl hydroperoxide.

[c] PAA is peroxyacetic acid.

Table S2: The differences between the measured (C_{aq}^{m}) and predicted (C_{aq}^{t}) liquid-phase H_2O_2 levels for the three types of seven rain events.

Types	Date	Rain intensity (mm h^{-1})	Number of samples	Number of samples ($C_{aq}^{m} > C_{aq}^{t}$)	$C_{aq}^{m} - C_{aq}^{t}$ (μM)
I[a]	6 August	0.9	4	2	4.25
II[a]	30 August[b]	2.5	5	5	40.19
	24 July	5.2	10	6	7.09
	1 September	5.5	14	9	10.49
	8 August	6.9	7	7	14.71
III[a]	25 July	14.7	8	8	39.00
	5 August	22.6	4	3	29.91

[a] Types I, II, and III refer to rain intensity < 1 mm h^{-1}, 1−10 mm h^{-1}, and > 10 mm h^{-1}, respectively.

[b] The relationship between rain intensity and the difference between C_{aq}^{m} and C_{aq}^{t} ($C_{aq}^{m} - C_{aq}^{t}$) was abnormal on 30 August, and there may be several reasons influencing the liquid-phase H_2O_2 concentration.

Table S3: Summary of aerosol-phase H_2O_2 concentration in previous studies.

Region	Time	Aerosol-phase H_2O_2	Aerosols diameter	Extraction method	References
Niwot Ridge, Colorado, USA	24 July−4 August 1989	< 0.01−10 ng m^{-3}	/	soaking for > 30 min	Hewitt and Kok, 1991
UCLA, Los Angeles, CA, USA	May−August 2001	0−13 ng m^{-3}	< 10 μm	gentle agitation for several hours	Hasson and Paulson, 2003
UCLA, Los Angeles, CA, USA	after 6 May 2004	0.58 ± 0.30 ng μg^{-1}	< 2.5 μm	gentle agitation for 2 h	Arellanes et al., 2006
Freeway, Los Angeles, CA, USA	prior to 6 May 2004	0.42 ± 0.30 ng μg^{-1}	< 2.5 μm	gentle agitation for 2 h	Arellanes et al., 2006
Upwind Riverside, CA, USA	2−10 August 2005	0.48 ± 0.32 ng μg^{-1}	2.5−10 μm	immersing filters for 2 h	Wang et al., 2010
Downwind Riverside, CA, USA	23 June− 28 August 2008	0.37 ± 0.18 ng μg^{-1}	2.5−10 μm	immersing filters for 2 h	Wang et al., 2010
Fresno, California, USA	2006−2009	0.59 ± 0.32 ng μg^{-1}	< 2.5 μm	shaking in the dark for 4 h	Shen et al., 2011
UCR, Riverside, CA, USA	2−10 August 2005	0.95 ± 0.69 ng μg^{-1}[a]	< 2.5 μm	immersing filters for 2 h	Wang et al., 2012
CRCAES, Riverside, CA, USA	23 June− 28 August 2008	0.49 ± 0.55 ng μg^{-1}[a]	< 2.5 μm	immersing filters for 2 h	Wang et al., 2012
UCLA, Los Angeles, CA, USA	2009−2010	0.11 ± 0.07 ng μg^{-1}	< 2.5 μm	immersing filters for 2 h	Wang et al., 2012
Taipei, China	July−September 2000	0.68 ng μg^{-1}[b]	0.18−1 μm	ultrasonication for 10 min	Hung and Wang, 2001
Rubidoux, CA, USA	July 2003	243 ng m^{-3}[b]	/	ultrasonication for 15 min	Venkatachari et al., 2005
Austin, Texas, USA	November 2011 −September 2012	42.5 ± 37.4 ng m^{-3}[b]	/	sonication for 10 min	Khurshid et al., 2014
Beijing, China	21 December 2018 −5 January 2019	0.093 ± 0.085 ng μg^{-1}	< 2.5 μm	shaking in the dark for 15 min	This study

[a] Samples were sporadically contaminated from Virtual Impactors, thus, the aerosol phase H_2O_2 level may be above the actual value.

[b] The values are ROS concentrations. ROS concentrations include other reactive oxygen species besides H_2O_2.

Table S4: The estimated averages of reaction rate (RR) and sulfate formation rate (SFR) during a sever haze event on 2−3 January 2019.

H_2O_2 level	RR (mol m^{-3} h^{-1})	SFR (μg m^{-3} h^{-1})
Measured_H_2O_2	3.03×10^{-9}	0.29
Predicted_H_2O_2[a]	6.28×10^{-12}	6.02×10^{-4}

[a] Predicted_H_2O_2 is calculated using Henry's law.

Table S5: The ratio of the maximum to initial H_2O_2 concentration (C_{max}/C_0) in the extracted solution and molar concentration ratio of aerosol-phase TPOs to H_2O_2 for the three types.

Samples	Types	Date[a]	C_{max}/C_0	Molar concentration ratio of TPOs/H_2O_2
1	First type	29 December _D	1.56	4.78
2		29 December _N	1.48	5.71
3	Second type	31 December _N	33.68	34.45
4		1 January _D	44.76	45.67
5	Third type	2 January _D	1.00	44.37
6		2 January _N	1.00	50.80

[a] _D and _N represent samples collected at day-time and night-time, respectively.

Table S6: The average values of meteorological parameters, trace gases, $PM_{2.5}$ and TPOs for the three types during BJ-2018Winter.

Parameters	Samples 1 and 2[a]	Samples 3 and 4[b]	Samples 5 and 6[c]
T (°C)	269	269	271
RH (%)	14.10	26.37	30.33
WS (m s^{-1})	1.96	1.33	0.50
CO (ppbv)	300.65	647.44	1065.88
SO_2 (ppbv)	1.40	3.45	6.50
NO (ppbv)	1.19	23.84	44.80
NO_2 (ppbv)	17.03	27.03	40.23
O_3 (ppbv)	23.33	15.43	8.99
$PM_{2.5}$ (μg m^{-3})	13.45	37.30	63.11
TPOs (ng m^{-3})	108.50	311.75	379.16
TPOs (ng μg^{-1})	6.54	8.27	5.56

[a] Samples 1 and 2 (the first type) were collected on 29 December 2018.

[b] Samples 3 and 4 (the second type) were collected on 31 December 2018−1 January 2019.

[c] Samples 5 and 6 (the third type) were collected on 2 January 2019.

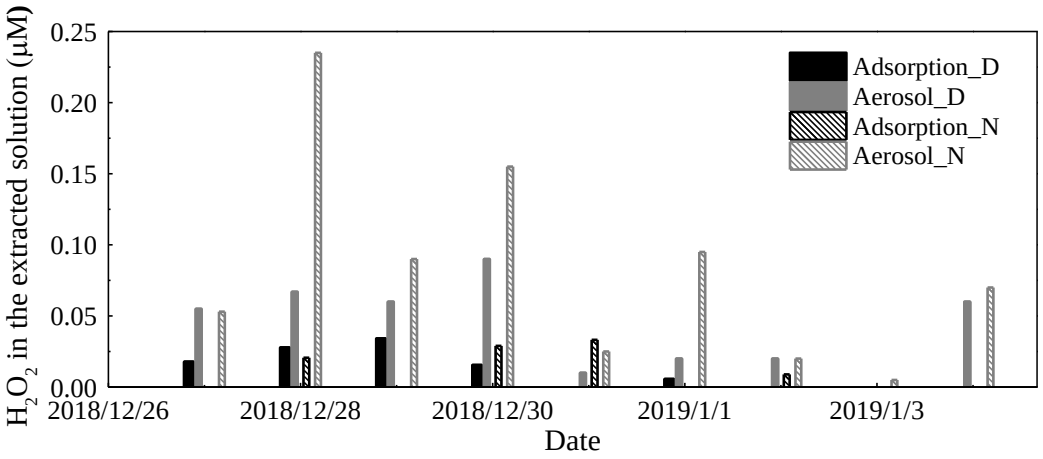

350

Figure S1: The concentrations of H_2O_2 in adsorption and aerosol samples in the extracted solution from 27 December 2018 to 4 January 2019. _D and _N denote samples collected at day-time and night-time, respectively.

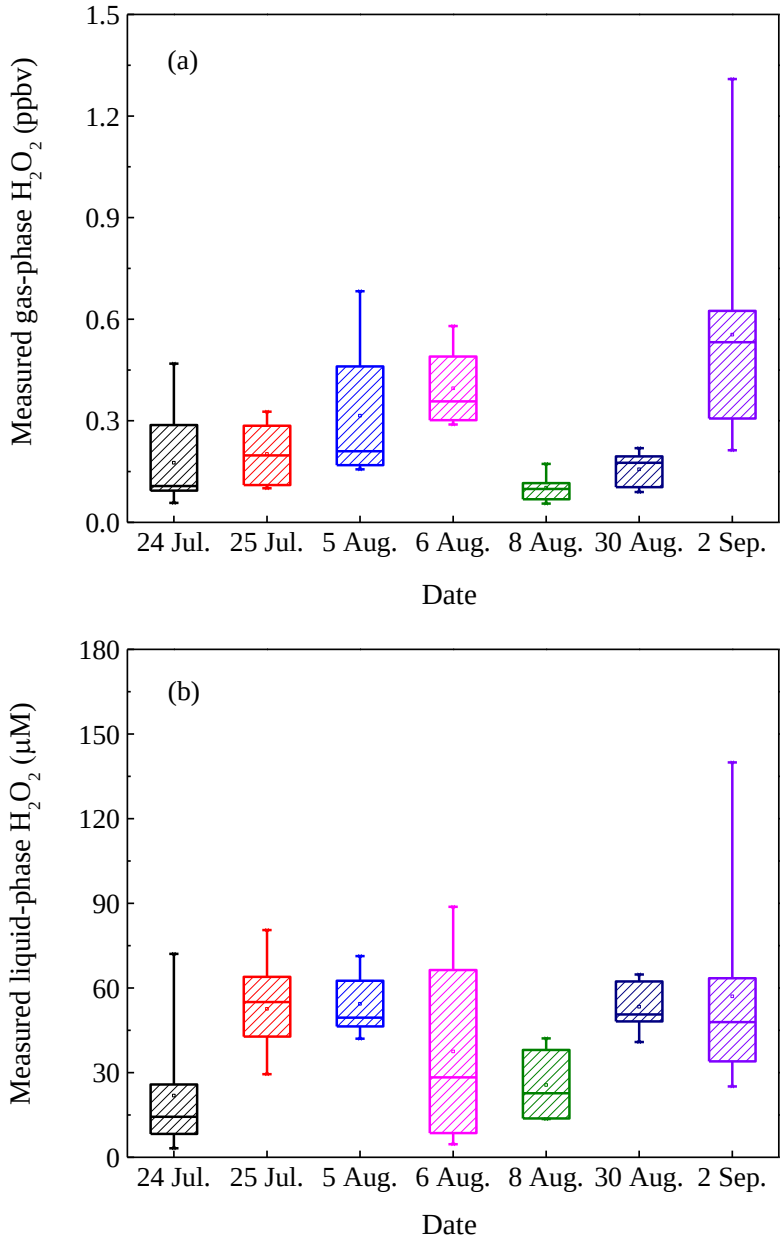

355

Figure S2: Concentrations of the measured (a) gas-phase and (b) liquid-phase H_2O_2 in seven rain episodes during BJ-2018Summer. Colors represent rain episodes by date. Box ranges represent 25 % and 75 % concentrations of H_2O_2, whisker ranges denote minimum and maximum values of H_2O_2, and middle square in the box denotes the mean value of H_2O_2.

360

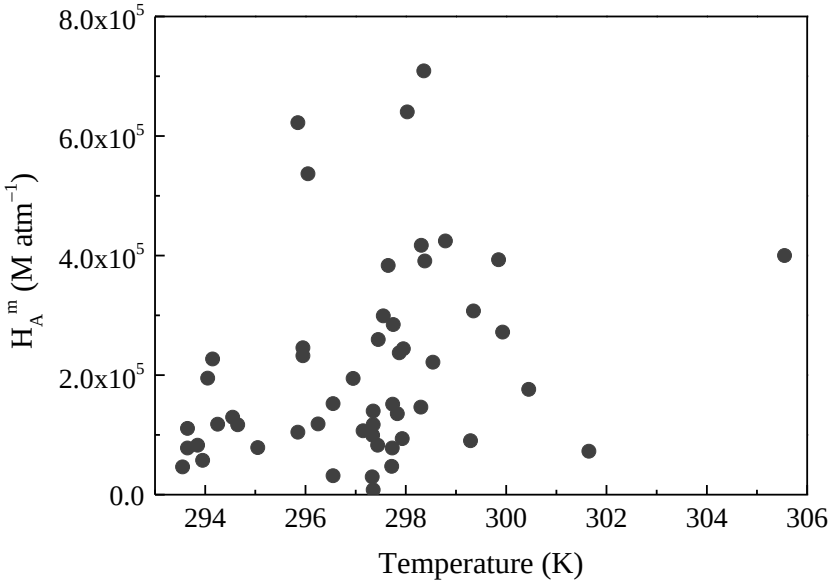

Figure S3: The variation of effective field-derived Henry's law constant (H_A^m) with temperature in seven rain episodes.

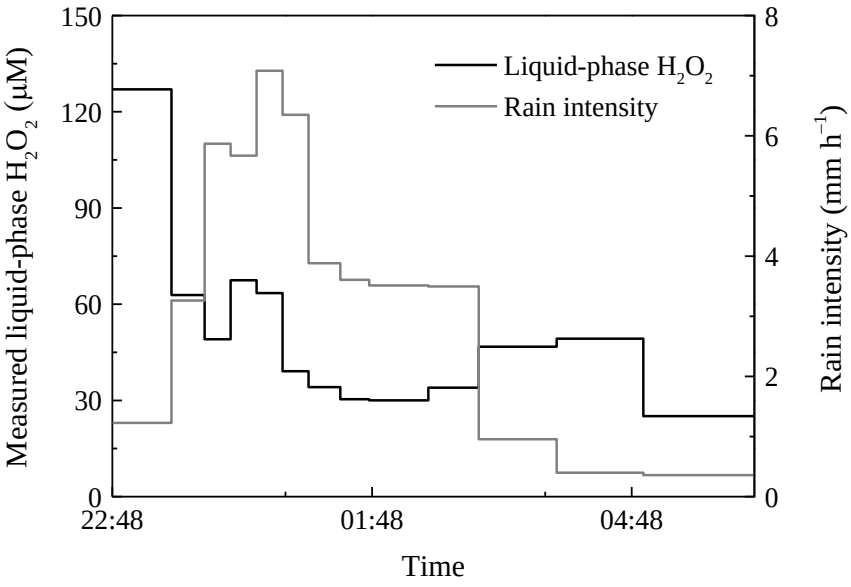

365

Figure S4: The relationship between the measured liquid-phase H_2O_2 level (left axis) or rain intensity (right axis) and time on 1−2 September 2018.

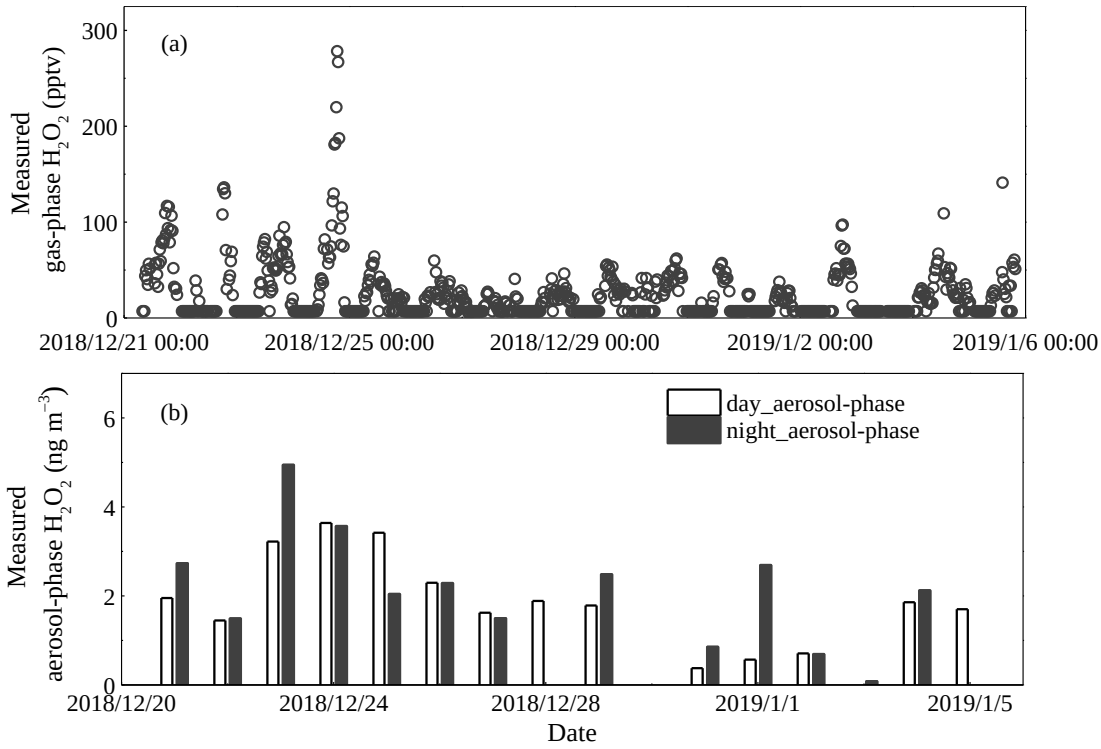

370 **Figure S5**: Measured concentrations of (a) gas-phase and (b) aerosol-phase H_2O_2 during BJ-2018Winter. Day_aerosol-phase and night_aerosol-phase represent samples collected at day-time and night-time, respectively.

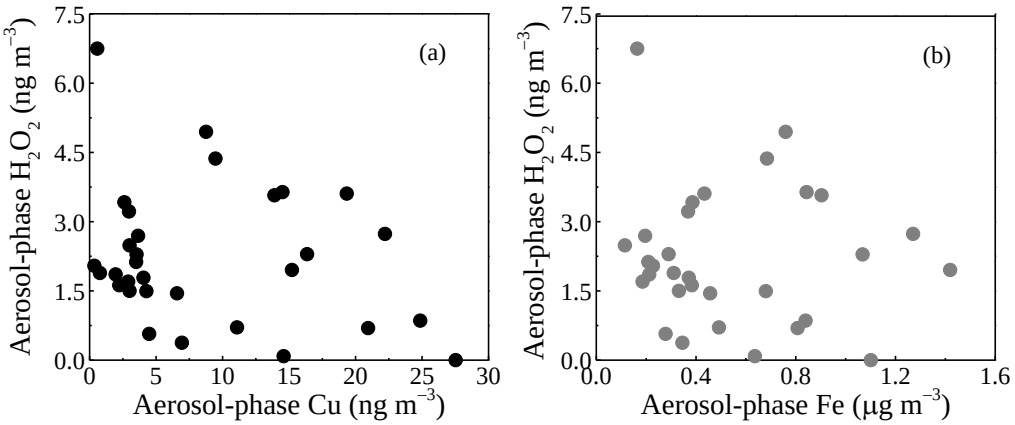

375 **Figure S6:** The dependency of measured H_2O_2 concentration on levels of (a) Cu and (b) Fe in aerosols.